



# Structure-activity relationships of Ni-Cu/Al<sub>2</sub>O<sub>3</sub> catalysts for $\gamma$ -valerolactone conversion to 2-methyltetrahydrofuran

Iker Obregón\*, Inaki Gandarias, Ainhoa Ocio, Iker García-García, Nerea Alvarez de Eulate, Pedro L. Arias

*Department of Chemical and Environmental Engineering, Faculty of Engineering, University of the Basque Country (UPV/EHU), Alameda Urquijo s/n, 48013 Bilbao, Spain*

## ARTICLE INFO

### Article history:

Received 21 December 2016  
Received in revised form 24 March 2017  
Accepted 1 April 2017  
Available online 2 April 2017

### Keywords:

2-Methyltetrahydrofuran  
 $\gamma$ -valerolactone  
Biofuel  
Hydrogenolysis

## ABSTRACT

The activity of a series of impregnated Ni-Cu/Al<sub>2</sub>O<sub>3</sub> catalysts was evaluated for the production of 2-methyltetrahydrofuran (MTHF) from  $\gamma$ -valerolactone using 2-butanol as solvent. These catalysts evidenced that their activities depend more on the metal phase nature than on the metal sites dispersion, achieving three times higher Normalized MTHF Productivity (NMP) the samples with the highest amounts of the Ni-Cu alloy. In addition, the activity of those high Ni-Cu alloy containing samples showed to be limited by their low surface acidity. The promotion of the alloy formation, acidity and metal-acid sites proximity was achieved by a co-precipitation method. This new catalyst, calcined and reduced at 450 °C, allows a MTHF yield of 64% after 5 h. The tested catalysts showed deactivation by carbon deposition which could be overcome by intermediate regeneration between runs. The best catalyst showed stable > 54% MTHF yield for three consecutive runs.

© 2017 Elsevier B.V. All rights reserved.

## 1. Introduction

The development and exploitation of renewable energy sources and vectors is an issue of great importance for nowadays societies in order to reduce their dependency on more pollutant traditional energy resources. Triggered by the transportation sector, crude oil is the most consumed energy feedstock with 33% of global energy share [1]. Different alternatives have been proposed for this sector, such as hydrogen cells or fully electrical vehicles, however, biomass derived fuels are the most straightforward alternative since existing infrastructures and vehicle engines could be used. Biomass is considered a suitable, sustainable and widespread substitute for the highly localized and finite fossil fuel feedstocks. In addition to a higher energy independence, further benefits of biomass utilization for fuel and fine chemicals production include a reduced carbon footprint of the products [2] owing to a potentially closed carbon cycle (Fig. 1). Nevertheless, the successful switch from our petrol based economy to a biomass based energy model requires the development of new catalytic processes to upgrade platform molecules derived from lignocellulose through cost effective ways.

In this context, levulinic acid (LA) is a highly interesting building block molecule due to the ease of its industrial scale production [3,4] and the wide range of added-value products that can be synthesized from it: pharmaceuticals, solvents, monomers and transportation fuels among others [3,4]. Besides, it can easily react to products such as  $\gamma$ -Valerolactone (GVL), which was proposed as an ideal liquid fuel because of its properties such as high flash point, low toxicity and suitable octane number [5,6]. However, the high water solubility of this molecule hampers its use in currently used gasoline engines. In order to overcome this drawback, GVL can be further hydrogenolysed to produce 2-methyltetrahydrofuran (MTHF), a molecule with interesting fuel properties (similar mileage, RON, etc.) and very low water solubility, which makes its implementation in nowadays gasoline facilities and engines straightforward. In addition to its use as a fuel, MTHF is also considered as an ideal green solvent with a broad applicability range and increasing industrial presence in important sectors such as the pharmaceutical one [2,7].

Despite the interest of this chemical, MTHF production from LA is scarcely reported in the literature. The hydrogenation of LA to the intermediate GVL is a fast and easy reaction [8,9], but the high stability of this molecule makes its conversion to MTHF challenging. Therefore, in order to develop active catalysts for MTHF production the attention should be focused on their activity for GVL conversion. This reaction starts with the addition of

\* Corresponding author.

E-mail address: [iker.obregon@ehu.eus](mailto:iker.obregon@ehu.eus) (I. Obregón).

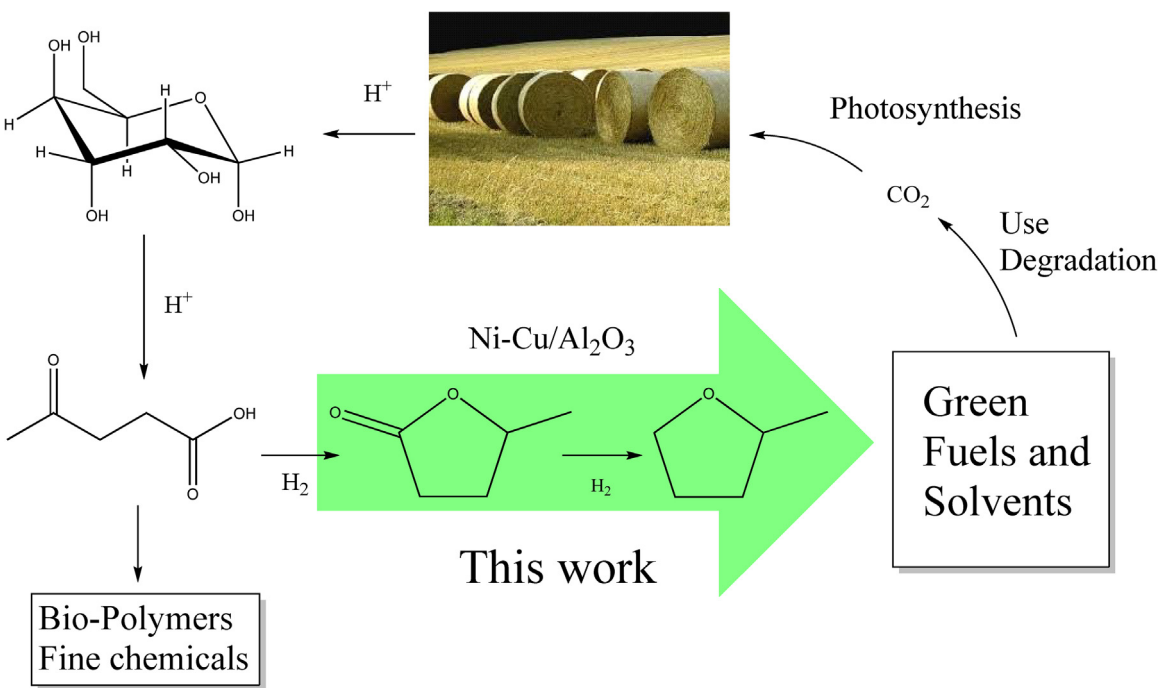


**Fig. 1.** Biofuel and CO<sub>2</sub> integrated cycle.

two hydrogen molecules to produce 1,4-pentanediol (PDO) which, upon dehydration/intramolecular etherification, yields MTHF. The described hydrogenation-dehydration reaction sequence requires both hydrogenating and acid catalyst functionalities [10–12].

The highest reported MTHF yields from (LA and) GVL using heterogeneous catalysts were achieved using both noble [13,14] and non-noble [15–17] metal based bi-functional catalysts. Nevertheless, the future biofuel production to be economically viable requires the use of inexpensive catalysts based on highly available transition metals. In this regard, catalysts based on bimetallic Ni-Cu are documented to yield some of the highest MTHF yields [9,15,17,18]. Previous investigations explored the role of the total metal loading on SiO<sub>2</sub> based catalysts [15], and important promotion effects were observed on bimetallic Ni and Cu catalysts both supported on SiO<sub>2</sub> and Al<sub>2</sub>O<sub>3</sub> [15,17]. In addition to the heavy influence of the metallic phase [17,19,20], the support material [14,16,20], their interactions [15,17,19,21] and the preparation method are reported to greatly affect the GVL conversion. Therefore, in order to rationally design optimized Ni-Cu/Al<sub>2</sub>O<sub>3</sub> catalysts for the production of MTHF, the structure-activity relationships need to be set and understood, *i.e.* the role of the metal sites, the relevance of the Ni-Cu interactions and the effect of the catalyst acidity. To achieve this goal, the effect of the total metal content and the catalyst preparation technique was analyzed. Finally, stability studies of the optimized catalyst, along with a detailed characterization, are also shown.

2-butanol (2-BuOH) was selected as solvent for this reaction based on the following criteria: *i)* to the best of our knowledge, aqueous phase PDO or MTHF production has only been published using promoted noble metal catalysts [14,19,20,22] and water was reported to negatively affect the activity of base metal catalysts [17]; *ii)* 2-BuOH can be used for LA separation from the biomass hydrolysis aqueous solution in a nicely engineered process [23–25]; and *iii)* GVL conversion to MTHF was reported to require high hydrogen availabilities which can be provided by a combination of H<sub>2</sub> pressure and a suitable hydrogen donor solvent [9], such as secondary alcohols. Besides, the fact that 2-BuOH can be used as fuel significantly reduces the product purification requirements, improving the process economy.

## 2. Experimental

### 2.1. Catalyst synthesis

Impregnation catalysts were prepared as previously reported [8]. Briefly, the desired amounts of γ-Al<sub>2</sub>O<sub>3</sub> (Alfa-Aesar) were mixed with deionized water in a 1:9 weight ratio and the proper amounts of metal precursor salts (Ni(NO<sub>3</sub>)<sub>2</sub>·6H<sub>2</sub>O, Sigma-Aldrich and Cu(NO<sub>3</sub>)<sub>2</sub>·5/2H<sub>2</sub>O, Alfa-Aesar) were added and stirred overnight at 90 rpm. Water was removed by heating the solution to 60 °C under vacuum.

Sequential impregnation catalysts were prepared following the same procedure but only one of the metal precursor salts was added to the solution. Water was removed under vacuum and the powder was crushed and calcined. The so obtained powder was, then, impregnated with the other metal precursor salt following the same procedure.

Co-precipitated catalyst were prepared according to a previously reported procedure [26]. Briefly, calculated amounts of metal precursor salts were dissolved in deionized water so that the concentration was 0.5 mol/L. The solution was then added drop-wise to 200 mL of deionized water under 500 rpm stirring while keeping the pH of the solution fixed at 7.0 by concentrated NH<sub>4</sub>OH addition. The formed slurry was then aged overnight at 60 °C and vacuum filtered.

All the catalysts were dried overnight at 110 °C, crushed to <450 μm particle size and calcined at 300 °C for 2 h (2 K/min ramp). Prior to activity tests, the catalysts were reduced at 450 °C (10 K/min heating ramp) for 1 h under H<sub>2</sub> flow and cooled down under N<sub>2</sub> flow. Activated catalysts were stored under isoctane to prevent contact with air.

### 2.2. Activity tests

Activity tests were carried out in 50 mL Hastelloy autoclaves with a magnetic stirrer and a glass liner. The typical reaction mixtures consisted of 5.3 g of a 5 wt% GVL in 2-butanol with a substrate/catalyst weight ratio of 10. The autoclaves were filled with the reduced catalysts and the reaction mixture, sealed, flushed

three times with H<sub>2</sub>, loaded with 50 bar H<sub>2</sub>, placed in preheated heating plates at 230 °C, and stirred at 500 rpm for 5 h. At the end of the reaction, the stirring was stopped, the autoclaves were cooled down, and the pressure in the autoclaves was slowly released. The catalyst was separated from the reaction mixture by centrifugation and liquid samples taken for GC analysis with 2-hexanol as external standard.

For reusability experiments the separated catalyst samples were stored under isoctane avoiding contact with air until the next activity experiment. The catalyst samples to be reused with intermediate treatments were identically handled and reduction or calcination and reduction steps were applied before the next activity test depending on the case. Noteworthy, no differences on the visual aspect were observed between the fresh, used and regenerated samples.

### 2.3. Elemental analysis (ICP-OES)

The metal content of the catalysts was measured by inductively coupled plasma-optical emission spectroscopy (ICP-OES) on a Perkin Elmer Optima 2000 OV device. Prior to the analysis samples were digested in a mixture of HCl, HNO<sub>3</sub>, and HF using an ETHOS 1 Advanced Microwave Digestion System.

### 2.4. Temperature programmed reduction (TPR)

The weighted, non-activated, catalyst samples were placed in a U shaped quartz cell and subjected to temperature programmed reduction (TPR) in the cited AutoChem II instrument (Micromeritics) equipped with a calibrated TCD detector. The measurements were carried out at a 10 K/min heating rate up to 1000 °C with 50 mL/min gas flow of a 5 vol% H<sub>2</sub> mixture in Ar while monitoring H<sub>2</sub> consumption.

### 2.5. NH<sub>3</sub> temperature programmed desorption (NH<sub>3</sub>-TPD)

Ammonia temperature programmed desorption was carried out in an AutoChem II (Micromeritics) device. The weighted, non-activated, samples were placed in a U shaped quartz cell, reduced with the temperature program used prior to the activity tests, saturated with 50 mL/min of a 10 vol% NH<sub>3</sub> in He gas flow for 30 min at 100 °C and then flushed with He at 150 °C for 60 min to remove the physically adsorbed NH<sub>3</sub>. The samples were then heated to 900 °C by a 10 K/min ramp while monitoring NH<sub>3</sub> release by means of a calibrated TCD detector.

### 2.6. CO chemisorption

CO chemisorption was carried out in an AutoChem II (Micromeritics) device equipped with a calibrated TCD detector. The weighted, non-activated, samples were placed in a U shaped quartz cell, reduced with the same temperature program used for the activation of the catalyst, flushed with He and cooled down to 35 °C. At this temperature CO pulses, 0.01778 cm<sup>3</sup> of a 5 vol% CO in He mixture, were injected to the sample until saturation was observed. As this technique allows no differentiation between the CO chemisorbed on Ni and Cu, only the total CO uptake (μmol CO/g catalyst) will be considered.

CO chemisorption was used to calculate the normalized MTHF productivity (NMP) of the catalyst, defined as the ratio between the produced MTHF moles and the metal sites moles on the catalyst (determined by CO chemisorption) and the reaction time (Δt), according to Eq. (1).

$$NMP = \frac{mol_{MTHF}}{g_{Cat} (mol_{CO}/g_{Cat}) \Delta t} \quad (1)$$

### 2.7. X-ray diffraction (XRD)

Reduced samples were stored under isoctane to avoid oxidation and handled avoiding contact with air and analyzed by XRD in an Xpert PRO device equipped with a Bragg-Brentano goniometer and a Cu cathode working at 40 kV and 40 mA. The spectra were recorded in the 10°–80° 2θ range with a 0.026 step size.

High resolution XRD data were collected on a Bruker D8 Advance diffractometer equipped with a Cu tube, Ge(111) incident beam monochromator ( $\lambda = 1.5406 \text{ \AA}$ ) and a Sol-X energy dispersive detector. The sample was mounted on a zero background silicon wafer embedded in a generic sample holder. Data were collected from 40° to 50° 2θ (step size 0.01 and time per step of 517 s) at room temperature. A fixed divergence and antiscattering slit 1° giving a constant volume of sample illumination were used.

The obtained XRD patterns were compared with the powder diffraction files (PDF) by Xpert-Pro Score tool.

### 2.8. Scanning transmission microscopy (STEM)

Scanning TEM images were obtained on a TECNAI G2 20 TWIN operated at 200 kV and equipped with LaB<sub>6</sub> filament, EDAX energy dispersive electron spectroscopy (EDS) microanalysis system and high angle annular dark-field-scanning transmission electron microscopy (HAADF-STEM). Samples used for TEM analysis were prepared via dispersion into octane solvent and keeping the suspension in an ultrasonic bath for 15 min, after which a drop of suspension was spread onto a TEM molybdenum grid (300 Mesh) covered by a holey carbon film followed by drying under vacuum.

### 2.9. X-ray photoelectron spectroscopy (XPS)

XPS spectra of the reduced catalysts were obtained on a VG Escalab 200R spectrometer equipped with a hemispherical electron analyzer and a Mg Kα ( $h\nu = 1253.6 \text{ eV}$ ) X-ray source. Binding Energy (BE) values were referred to C1s peak at 284.6 eV. Reduced samples were stored under isoctane to avoid oxidation prior to analysis and handled avoiding contact with air.

## 3. Results and discussion

### 3.1. Effect of the metal content

In order to study the effect of the total metal content, a series of catalysts with the optimized Ni:Cu weight ratio (2:1) determined in a previous work [17], and different total metal loadings were prepared by a Wet Impregnation (WI) method and their activity was tested. The results displayed in Fig. 2 showed, as expected, the negligible activity of the bare γ-Al<sub>2</sub>O<sub>3</sub> support for this reaction, owing to the lack of hydrogenating active sites. For metal loads up to 35% the activity of the catalysts increased with the metal content, reaching a maximum 48% MTHF yield. Further increase on the metal loading to 50% showed no significant differences compared to the 35% catalyst. Carbon balances (CB) were typically above 90% and the selectivity of the catalysts increased with the metal loading, from 66% for the 10WI catalyst up to 80% on the 50WI. In addition to the substrate, GVL, and MTHF, other detected reaction products were valeric acid and its butyl ester (2–3%), 1- and 2-pentanol (1–1.5%) and PDO (<1.5%).

Catalyst characterization was conducted in order to determine the origin of the activity differences. Since the reaction consists of hydrogenation and dehydration steps, both metallic and acidic active sites are required. Therefore, NH<sub>3</sub>-TPD and CO chemisorption experiments were performed on freshly reduced catalysts (Table 1).

Interestingly, the 10WI catalyst showed a higher acidity than the bare γ-Al<sub>2</sub>O<sub>3</sub> support, suggesting that a part of the added metals

**Table 1**

Peak area percentage from fitting of the TPR profiles in Fig. 3a), acidity quantification from the profiles in Fig. 3b) and CO chemisorption results for WI catalysts with different metal loads.

Catalyst	TPR			NH <sub>3</sub> -TPD (mmol NH <sub>3</sub> /g)			CO (μmol/g)
	% Peak 1 <sup>[a]</sup>	% Peak 2 <sup>[a]</sup>	% Peak 3 <sup>[a]</sup>	150–525 °C	525–900 °C	Total	
Al <sub>2</sub> O <sub>3</sub>	–	–	–	0.51	0.61	1.12	–
10WI	77 (312)	–	23 (558)	0.84	0.79	1.63	65.6
20WI	65 (216)	7 (280)	28 (416)	0.48	0.44	0.91	90.5
35WI	60 (226)	26 (278)	14 (405)	0.48	0.37	0.85	37.5
50WI	64 (218)	30 (251)	6 (384)	0.41	0.33	0.73	44.8

<sup>[a]</sup>The figures in brackets indicate the temperature (°C) of the reduction peaks maximum. TPR fitting are shown in Fig. A1 in the Appendix.

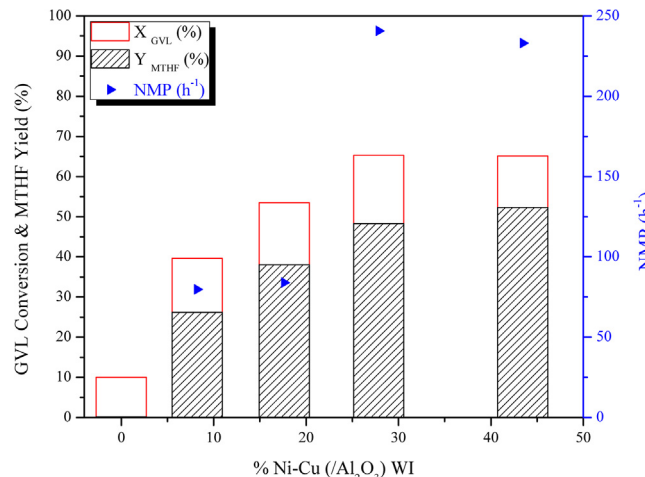


**Fig. 2.** GVL conversions, MTHF yields and NMP (h<sup>-1</sup>) for 2:1 Ni-Cu catalysts with different total metal loadings. Reaction conditions: 230 °C, 50 bar H<sub>2</sub> pressure (@roomT), GVL-to-Cat. weight ratio of 10, 5 wt% GVL in 2-butanol, 500 rpm stirring and 5 h reaction time. NMP is calculated as the MTHF mol produced per metal active site (CO chemisorption) and reaction time.

was not reduced during the activation, probably leading to Ni oxide phases which can act as Lewis acid sites [27]. Further increases in the metal loading led to a steady decrease in the total acidity of the material from 0.91 to 0.73 mmol NH<sub>3</sub>/g (Table 1).

CO chemisorption showed an increasing amount of metallic active sites with metal loadings up to 20% (Table 1). Further increases in the metal loading led to a sharp decrease in the metallic sites amount. These measurements are consistent with XRD patterns of the reduced catalysts, which showed no Ni or Cu reflections for loadings below 35% and important metal related reflections for the higher metal loads (Fig. 3c)). These two techniques consistently indicated that the catalysts with lower metal contents contained small and dispersed metal particles while the highly loaded ones showed larger particles.

TPR profiles of the catalysts (Fig. 3a)) showed three differentiated peaks which can be related to the different metal species *i.e.* Cu (peaks centered at 216–227 °C) [17,28], Ni in high interaction with the Al<sub>2</sub>O<sub>3</sub> support (peaks centered at 377–417 °C) [28,29] and a Ni-Cu alloy (shoulder-peak centered at 262–271 °C) [17]. The profile of the 10WI catalyst is considerably different from the others, showing two reduction peaks at 316 and 555 °C. The high T reduction peak can be ascribed to Ni aluminate species whereas the low T peak can be ascribed to Cu species [28].

A comparison of the fitted profiles evidenced a qualitative increase in the Ni-Cu interactions with increasing metal loadings, which enhanced the reducibility of the metal species [28,30] as indicated by the shift towards lower temperatures of all the reduction peaks (100 °C for the low T peak and up to 180 °C for the high T peak, Table 1). TPR profiles also confirmed the hypothesis of incomplete metal reduction, with reduction peaks at temperatures above

the catalyst activation temperature (450 °C). The unreduced metal fraction was the largest for the 10WI catalyst, and decreased to minimal amounts with the increment of the metal loading. As described in a previous publication [17], the presence of a Ni-Cu alloy can be observed in the second reduction peak located around 280 °C. This peaks contribution was the highest for the 50WI catalyst and decreased with the metal content until it was not detected on the 10WI catalyst.

All the described characterization along with the activity results suggest that the total amount of metal sites or acidic sites is not as influential for the activity of this catalyst series as the “specific activity” of the sites, as shown by the normalized MTHF productivity (NMP) in Fig. 2. Interestingly the NMPs of the metallic sites in the small particle containing catalysts, 10WI and 20WI, were almost equal and three times lower than the NMPs of the sites of the catalysts containing larger metal particles, *i.e.* 35WI and 50WI.

These results suggest that a stepwise change occurs in this catalysts surface chemistry when moving from small particles to larger clusters. Apparently, according to the presented activity and characterization data, particle agglomeration triggers the formation of the Ni-Cu alloy, whose active sites showed much higher activity than isolated Ni and Cu particles. However, the 50WI catalyst showed similar activity to the 35WI catalyst despite of the fact that the alloy was more abundant in the 50WI and the amount of metal sites was larger (Table 1).

Considering that the acidity was the only parameter that decreased from the 35WI to the 50WI catalyst it can be speculated that the catalyst acidity plays a role on the adsorption and activation of the GVL molecule aside from the dehydration of PDO to MTHF as shown in Fig. 4. The fact that only trace amounts of PDO were detected in the reaction media suggests that the PDO dehydration to MTHF is not the rate controlling step; hence, providing further evidence that the observed effect of the acidity is more strongly related to the conversion of GVL, the rate limiting step of the reaction, than it is for the dehydration of PDO.

According to these findings, it is reasonable to suggest that GVL may adsorb on an acid site and, due to this interaction, the GVL ring may lose some stability. As a result of the decreased stability, the addition of dissociated hydrogen atoms from adjacent metal (Ni-Cu) sites might become an easier process. This reaction mechanism, which is reported for other hydrogenolysis reactions [29,31], requires close proximity of metallic and acidic sites so that the GVL molecule can interact with both functionalities. A control experiment adding 50 mg of γ-Al<sub>2</sub>O<sub>3</sub> as an acid co-catalyst to a reaction with the 50WI catalyst demonstrated this point, since no activity differences were observed despite the increased in the total amount of acid sites on the reaction medium.

### 3.2. Sequential impregnation catalysts

In view of the importance of the Ni-Cu alloy, the acidity and their proximity, different impregnation procedures were applied trying to promote the formation of the Ni-Cu alloy along with

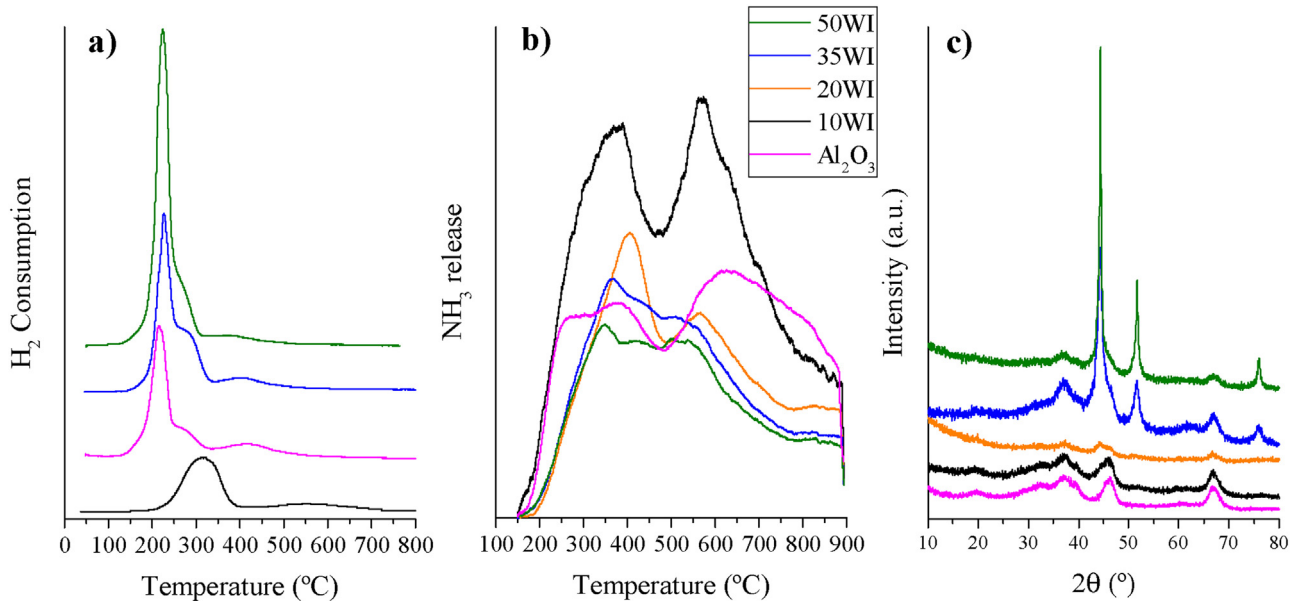


**Fig. 3.** a) TPR b) NH<sub>3</sub>-TPD and c) XRD profiles of the fresh WI catalysts with different metal contents. The signals in a) and b) are normalized by the weight of sample used for the analysis.

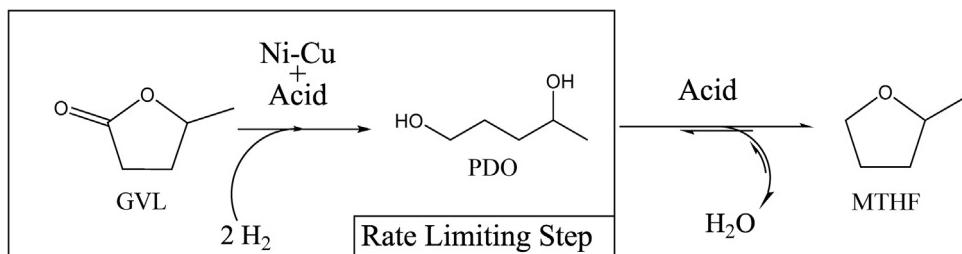


**Fig. 4.** GVL reaction mechanism and limiting step identification.

higher surface acidity. Based on the previously presented results the 35% metal content was selected (keeping the Ni-Cu weight ratio at 2) because it showed significant amounts of the Ni-Cu alloy and it showed higher acidity than the 50WI catalyst. Contrary to the simultaneous impregnation used to prepare the WI catalysts, sequential impregnation was used, alternating the order of the impregnation of Ni and Cu. The catalysts will be denoted as 35Ni + Cu, when Ni was the second impregnated metal, and 35Cu + Ni, when the second metal to be impregnated was Cu. The activity results for these catalysts are summarized in Fig. 5.

The activity data showed similar results for the three impregnation methods. The 35Ni + Cu catalyst showed a slight increase in the MTHF yield (53 vs. 48%) compared to the 35WI catalyst whereas the 35Cu + Ni showed similar values (47 vs. 48%) to those of the 35WI catalyst. As all the catalysts showed similar selectivity ( $\approx 75\%$ ), the same trend was observed regarding GVL conversion. In view of the slightly superior activity of the 35Ni + Cu catalyst, a metal content screening was carried out using this preparation method. The results, displayed in Fig. A2 (left), showed the 35% metal content to provide the highest activity and NMP.

TPR analysis of the different 35% impregnation catalysts showed similar profiles. Nevertheless, a shift towards higher reduction temperatures (from 225 to 258 °C in the low T peak and from 400 to 442 °C in the high T peak, Table 2) was noticed for the sequential impregnation catalysts, indicating stronger metal support interactions [30] (Fig. 6a)). These results are consistent with the two calcination steps involved in the preparation method. Nonetheless, all the profiles showed the shoulder-peak on the low temperature

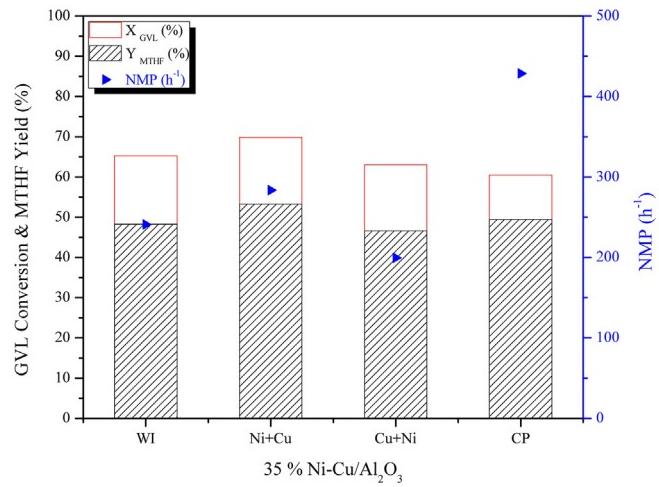


**Fig. 5.** GVL conversions, MTHF yields and NMP ( $\text{h}^{-1}$ ) of 35% Ni-Cu/Al<sub>2</sub>O<sub>3</sub> catalysts prepared by different methods.

peak, ascribed to the Ni-Cu alloy. In the sequential impregnation samples the Ni-Cu related peak was centered at 322–327 °C while on the 35WI it was centered at 278 °C.

TPR profile fitting showed that the highest amounts of the Ni-Cu alloy were present in the 35WI catalyst, followed by the 35Ni + Cu and the 35Cu + Ni showed the lowest amount (Table 2). These

**Table 2**

Peak area percentage from fitting of the TPR profiles in Fig. 6a), acidity quantification from the profiles in Fig. 6b) and CO chemisorption results for the 35% impregnation catalysts and the 20CP.

Catalyst	TPR			NH <sub>3</sub> -TPD (mmol NH <sub>3</sub> /g)			CO (μmol/g)
	% Peak 1 <sup>[a]</sup>	% Peak 2 <sup>[a]</sup>	% Peak 3 <sup>[a]</sup>	150–525 °C	525–900 °C	Total	
Al <sub>2</sub> O <sub>3</sub>	–	–	–	0.51	0.61	1.12	–
35WI	60 (226)	26 (278)	14 (405)	0.48	0.37	0.85	37.5
35Ni + Cu	71 (258)	19 (319)	10 (420)	0.44	0.41	0.85	40.1
35Cu + Ni	66 (253)	17 (303)	17 (434)	0.49	0.36	0.85	46.7
20CP	45 (233)	23 (263)	33 (515)	0.69	0.49	1.18	23.0

<sup>[a]</sup>The figures in brackets indicate the temperature (°C) of the reduction peaks maximum. TPR fitting are shown in Fig. A3 in the Appendix.

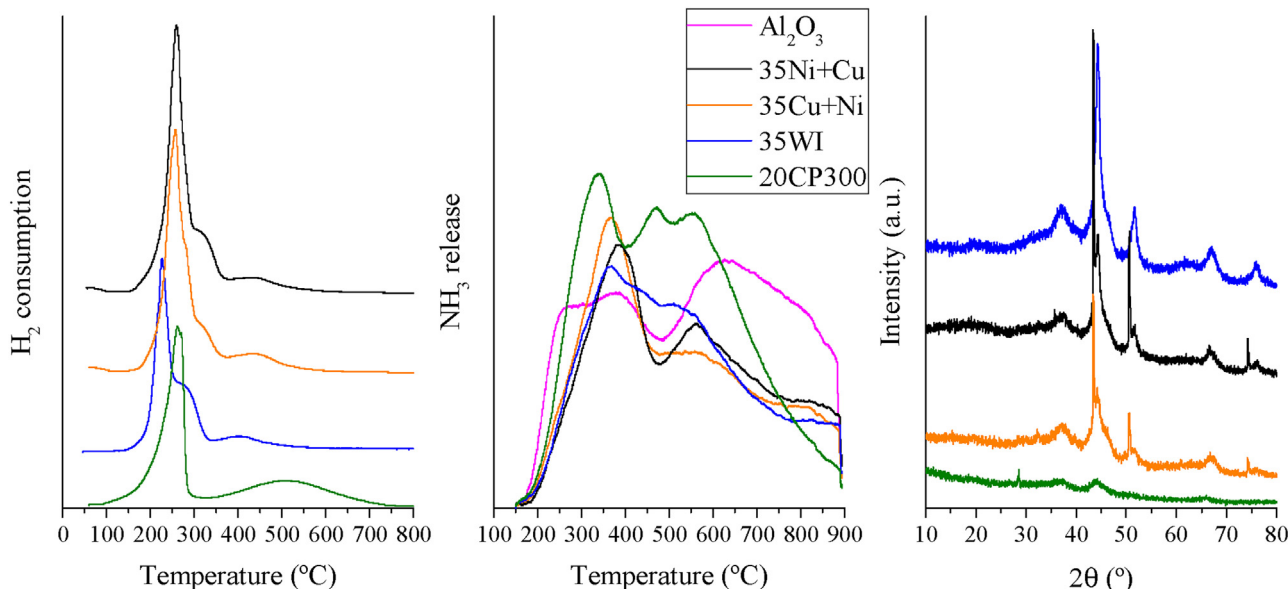


**Fig. 6.** a) TPR b) NH<sub>3</sub>-TPD and c) XRD profiles of the three impregnation method catalysts and the co-precipitated catalyst. The signals in a) and b) are normalized by the weight of sample used for the analysis.

results showed that no improvement was achieved by this impregnation procedure regarding the Ni-Cu alloy formation.

XRD patterns showed (Fig. 6c)), similarly to the 35WI catalyst, large Ni and Cu related reflections. In the case of the sequential catalysts, however, sharper Cu reflections were detected, indicating the presence of larger metal crystals. This fact is, again, consistent with the two calcination step procedure which promotes particle sintering. A closer look to the XRD patterns of the sequential impregnation catalysts revealed a meaningful asymmetry in the reflection related to Cu (43.3°, Fig. 6c)). High resolution XRD measurements of these samples allowed the detection of the reflection of the Ni-Cu solid solution, which was estimated to contain 9–14% Ni in Cu (Fig. A5). Considering the reference intensity ratio (RIR) corrected areas of the reflections ascribed to Ni, Cu and Ni-Cu respectively, it was estimated that the Ni-Cu solid solution was twice as abundant as the Cu phase in the 35Ni + Cu catalysts, whereas the opposite results were obtained for the 35Cu + Ni catalyst. These values do not fit with the estimations based on the TPR fitting showing similar Ni-Cu proportions. However, the different nature of the techniques may be responsible for this discrepancy. The smaller particle sizes found in the 35WI catalyst resulted in broader reflections that overlapped and, hence, phase analysis was not possible for this catalyst.

The NH<sub>3</sub>-TPD profiles of this catalyst series showed a similar total acidity, around 0.85 mmol NH<sub>3</sub>/g, but with differences regarding the strength distribution (Fig. 6b)). Despite the similar values observed in Table 2, the TPD profile showed the sequential impregnation catalysts to exhibit a larger acidity peak at low temperatures

(400 °C) while the WI (co-impregnated) catalyst showed higher amount of stronger acid sites (450–600 °C). These results suggest that, in this catalyst series, the acidity might be the activity limiting factor; owing to the fact that a series of catalysts with similar acidity and lower, yet high, Ni-Cu proportion and similar surface metal sites concentration (Table 2) showed similar activity results.

### 3.3. Co-precipitated catalysts

Considering the presented results, increased activity could be expected from catalysts prepared by a more efficient method [32] which enabled higher proportions of the Ni-Cu alloy along with higher surface acidity. Besides, the proximity of those two functionalities was found necessary for the conversion of GVL. Therefore, attempting to fulfill the mentioned requirements, another method was used to prepare a catalyst with the same Ni-Cu ratio and metal content. Nevertheless the actual metal content of this catalyst, prepared by a co-precipitation (CP) method was 20%, and it will be denoted as 20CP300 according to the used calcination temperature (in order to differentiate from other catalyst that will be presented in Section 3.4). This catalyst showed similar conversion and MTHF yield results compared to the 35% impregnated catalysts but with a noticeably higher NMP (1.8 times higher, Fig. 5). In addition, this catalyst also showed higher selectivity than the impregnated ones (81 vs. 75%). Similarly to the procedure applied to the Ni + Cu sequentially impregnated catalysts, a metal load screening was also carried out using the CP method (Fig. A2 right) and the 20% metal load (20CP300) showed the highest activity.

XRD profiles of the 20CP300 catalyst showed no reflections related to Ni or Cu phases and only small and broad  $\gamma\text{-Al}_2\text{O}_3$  related reflections (Fig. 6c)). The small particle size seems contradictory with the low metal active sites concentration (Table 2), however, it must be considered that the CO uptake of alloy catalysts may be significantly lower than that of non-alloyed catalysts [33]. Besides, the intimate contact between the metal and the support, facilitated by the CP method, could lead to unexposed metal particles on the bulk of the catalyst. The combination of these two factors could explain the low CO uptake of the CP catalyst. The close contact this method promotes is considered responsible for the superior activity of this catalyst; producing a balanced amount of acid and metallic active sites in close proximity from each other. As previously explained, this sites proximity is required for hydrogenolysis reactions [29,31] and for catalytic transfer hydrogenation (CTH) reactions [34], which were reported to be important in this reaction system [9].

The  $\text{NH}_3\text{-TPD}$  profile of the 20CP300 catalyst showed a significantly higher surface acid sites concentration in the low temperature range but most noticeably, in the high temperature region (Fig. 6b)). The TPR profile of the 20CP300 catalyst differs in shape from the previously presented ones: instead of a low temperature peak with a shoulder-peak, this profile shows a single peak with a tailing on the low temperature region. Peak fitting of the profile showed the presence of the aforementioned Cu, Ni-Cu and Ni phases (Fig. A3). In this case, high proportions of the Ni-Cu and the Ni aluminate phases were detected (Table 2), which fits the previously discussed preparation method effect of enhancing both alloy formation and metal-support interactions. These observations were further evidenced by the shift in the binding energy (BE) of Ni and Cu by XPS measurements.

As shown in Table 3, the BE of both Ni and Cu were consistently higher than the values observed for  $\text{Ni}/\text{Al}_2\text{O}_3$  and  $\text{Cu}/\text{Al}_2\text{O}_3$  samples respectively. The BE of Cu in Ni-Cu alloy is reported to increase by up to 0.3 eV [35,36], which is in good agreement with the results in Table 3. Consequently the BE of Ni in Ni-Cu alloys is reported to decrease by up to 0.5 eV [35,36]. Nevertheless, Ni interaction with the  $\text{Al}_2\text{O}_3$  support increases the BE of Ni by about 1.0 eV [37]. Considering those effects and the fact that the 20CP300 catalyst showed high amounts of Ni aluminate species (reduction peaks  $> 400^\circ\text{C}$ ),

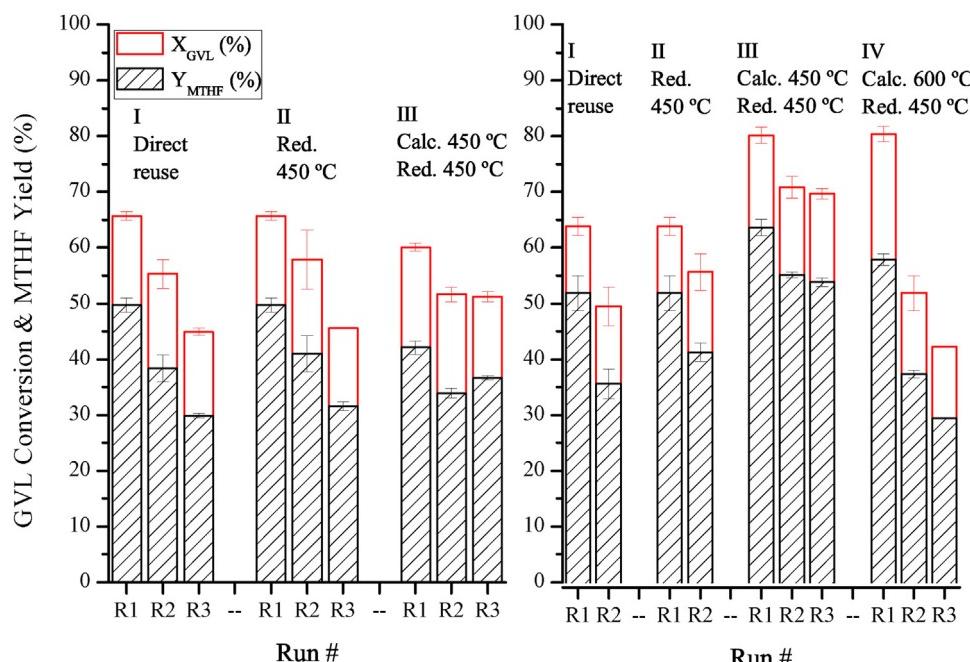


**Fig. 7.** Reusability experiments. Left graph corresponds to the 35Ni + Cu catalyst and the right graph to the 20CP catalyst.

**Table 3**

Surface atomic ratios and peak positions of fresh, used and regenerated 20CP samples calcined at different temperatures determined by XPS.

Catalyst	Sample	C/Al	Ni/Cu	Ni 2p <sub>3/2</sub> (eV)	Cu 2p <sub>3/2</sub> (eV)
20CP300 <sup>[a]</sup>	Fresh	0.26	2.76	855.7	933.3
	Fresh	0.29	3.07	855.6	933.5
	Used	0.44	3.31	855.6	933.5
	Solvent	0.35	2.94	854.9	933.2
	Regenerated	0.26	2.19	855.9	934.3
20CP600 <sup>[b]</sup>	Fresh	0.32	2.72	855.0	933.2
	Used	0.53	2.05	855.1	933.6
	Regenerated	0.15	2.48	854.6	933.5

<sup>[a]</sup>This sample was calcined at 450 °C, and this was also the regeneration temperature. <sup>[b]</sup>This sample was calcined at 600 °C, and this was also the regeneration temperature.

For reference purposes, the positions of the 2p<sub>3/2</sub> peaks of Ni and Cu in impregnated  $\text{Al}_2\text{O}_3$  catalysts were 854.8 and 933.0 eV respectively.

the increase in the Ni BE can be explained as the effect of the second interaction ( $\text{Ni}-\text{Al}_2\text{O}_3$ ) being more important on the Ni species than the first one (electronic interactions between Ni and Cu).

### 3.4. Catalyst stability and reusability

Reusability experiments were carried out with the most promising catalysts, i.e. 20CP300 and 35Ni + Cu, in order to assess the catalysts stability. As depicted in Fig. 7I, direct reuse of the catalyst led to a progressive activity decrease from around 50–36% MTHF yield from the first to the second run of both catalysts. Four reasons were speculated to be possible deactivation causes: i) metal leaching, ii) metal oxidation between runs, iii) poisoning by carbon deposition and iv) metal sintering.

Metal leaching was checked by measuring Ni, Cu and Al concentrations in the reaction mixture and they were found to be negligible (leached amount after 2 runs <0.2% in all cases, Table 4). After discarding this deactivation route, the influence of catalyst oxidation was tested by reducing the used catalysts between runs. As shown in Fig. 7II, no significant stability improvements were achieved with this strategy, suggesting that other deactivation mechanisms were more important under the applied conditions.

Next, the presence of carbon deposits was checked by XPS analysis of used catalysts, finding higher carbon contents on the used catalysts compared to the fresh samples (Table 3). In order to eliminate the possible carbon deposits through calcination a higher temperature than the one used for the original calcination step ( $300^{\circ}\text{C}$ ) is required. According to previous reports showing carbon combustion on catalysts used under similar reaction conditions [8,38–41],  $450^{\circ}\text{C}$  was chosen as the calcination temperature for catalyst regeneration. Consequently, fresh (uncalcined) catalyst samples were calcined at  $450^{\circ}\text{C}$  to avoid structural changes upon regeneration and the activities of these catalysts are displayed in Fig. 7III.

For the purpose of establishing whether the deposited carbon was produced out of the substrate (or reaction intermediates), from the solvent or from both sources, a control experiment was carried out exposing the 20CP450 catalyst, the 20CP catalyst calcined at  $450^{\circ}\text{C}$ , to the reaction conditions but in the absence of substrate (GVL) and then, reusing it for GVL conversion without any treatment. The results were significantly below of those achieved by the fresh catalyst (60 vs. 80% GVL conversion), suggesting that the carbonaceous deposit on the catalyst might be produced from the solvent as well as from the substrate or the reaction intermediates. This hypothesis was also confirmed by the increase in the carbon content of the catalyst determined by XPS (Table 3).

In order to confirm and overcome catalyst deactivation via carbon deposition, spent catalysts were calcined and reduced (regenerated) between runs. This strategy, as highlighted in Fig. 7III, provided catalyst stability but with important differences between the two catalysts. The 35Ni + Cu450 catalyst, calcined at  $450^{\circ}\text{C}$ , showed lower activity than the 35Ni + Cu catalyst calcined at  $300^{\circ}\text{C}$  (60 vs. 65% GVL conversion) and it further deactivated after the first use (51 vs. 60% GVL conversion). The third run of this catalyst, however, showed the same results as the second one. On the other hand, for the 20CP450 catalyst an improved activity was achieved after the new thermal treatment (77 vs. 61% GVL conversion). The second and third runs of this catalyst showed lower but stable activities with 70% GVL conversion and 54% MTHF yields (Fig. 7III right).

Similarly to the 35Ni + Cu450 catalyst, some deactivation took place from the first to the second runs of the 20CP450 catalyst and XPS analysis indicated that it was not related to remaining carbon deposits on the catalyst surface (Table 3); thus, the observed

**Table 4**  
Leaching metal analysis on the liquid media.

Cat	Run #	Conc. Liq. (mg/L)			Leached%		
		Al	Ni	Cu	Al	Ni	Cu
35 Ni + Cu	1	2.25	0.56	0.34	0.03	0.02	0.01
	2	0.85	1.78	0.78	0.01	0.07	0.04
				<b>Cumulative (%)</b>	<b>0.04</b>	<b>0.09</b>	<b>0.05</b>
35 CP	1	2.10	0.86	0.46	0.03	0.03	0.03
	2	0.52	0.69	0.83	0.01	0.03	0.09
				<b>Cumulative (%)</b>	<b>0.04</b>	<b>0.06</b>	<b>0.12</b>

**Table 5**

Summary of the NH<sub>3</sub>-TPD and CO chemisorption characterization of the CP samples. NH<sub>3</sub>-TPD profiles are showed in Fig. 9.

Catalyst	Sample	NH <sub>3</sub> (mmol/g)			CO ( $\mu\text{mol/g}$ )
		150–525 °C	525–900 °C	Total	
CP450	Fresh	0.92	0.20	1.12	52.1
	Used	0.86	0.40	1.26	57.3
	Regenerated	0.95	0.47	1.42	53.3
CP600	Fresh	0.97	0.32	1.29	42.6
	Used	1.03	0.64	1.67	62.8
	Regenerated	0.38	0.05	0.43	47.8

NH<sub>3</sub>-TPD results were divided into two temperature ranges for in order to provide further detail on the acidity variations.

deactivation must be related to structural or surfaces properties changes on the catalyst. Therefore, a calcination temperature of  $600^{\circ}\text{C}$  was tested for the 20CP catalyst looking for a higher structural stability. The freshly prepared 20CP600 showed to be as active as the fresh 20CP450, in good agreement with the similar acidity and metal sites concentration these catalysts presented (Table 5). However, a sharp and continuous activity decrease occurred in the second and third runs of this catalyst (Fig. 7IV).

XRD analysis of the used and regenerated 20CP450 and 20CP600 samples showed no differences (Fig. 8a)), indicating that both catalysts were structurally stable under the applied conditions. None of the patterns showed Ni or Cu related reflections, indicating that only small metal particles are present, and only broad Al<sub>2</sub>O<sub>3</sub> related reflections were detected.

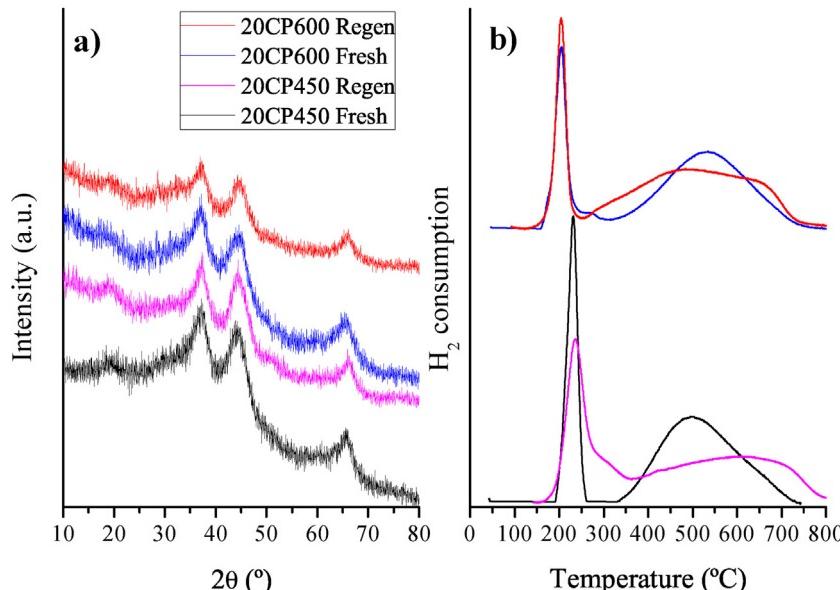


**Fig. 8.** a) XRD patterns and b) TPR profiles of the fresh and regenerated 20CP450 and 20CP600 catalysts.

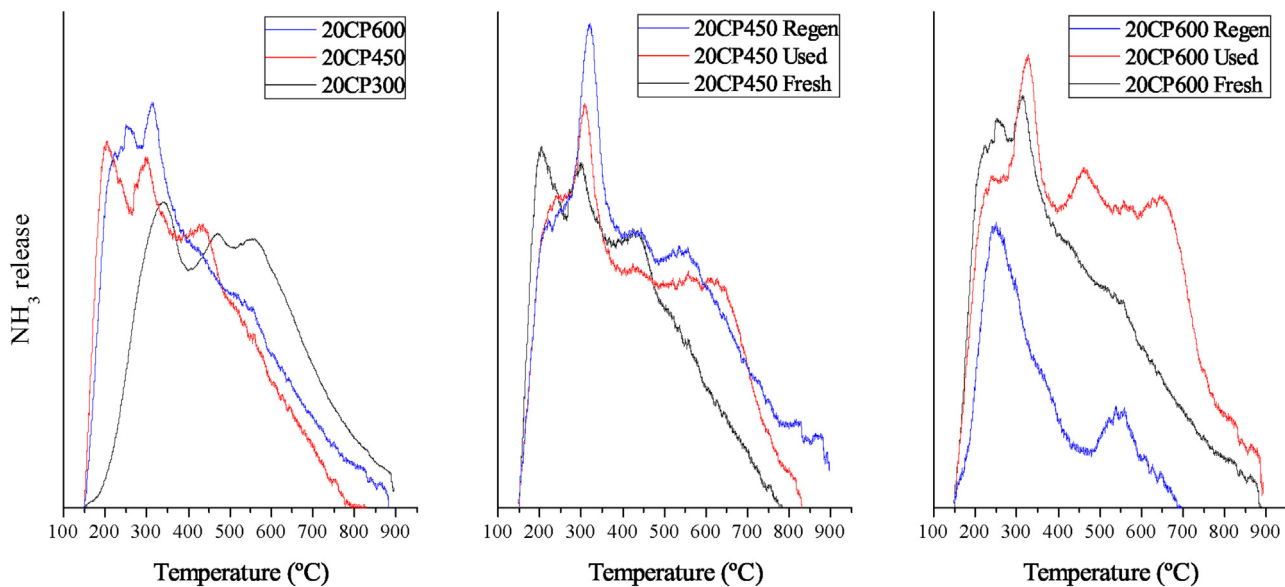


**Fig. 9.** NH<sub>3</sub>-TPD profiles. Fresh 20CP300, 20CP450 and 20CP600 catalysts (left graph). Center (20CP450) and right (20CP600) graphs show the profiles of fresh (black), used (red) and regenerated (blue) samples. (For interpretation of the references to colour in this figure legend, the reader is referred to the web version of this article.)

CO chemisorption analysis of the fresh, used and regenerated catalysts samples evidenced a similar behavior between the two catalysts (20CP450 and 20CP600). The used samples chemisorbed higher amounts of CO than the fresh samples, a fact previously reported in the literature [42–44]. The CO uptake of the regenerated samples decreased to values similar to that of the fresh sample in the case of 20CP450 and slightly higher in the case of the 20CP600 sample. These CO uptake variations can be ascribed to surface modification on the structure or the composition of the Ni-Cu alloy that may lead to different adsorption behaviors, in good agreement with the presented activity data. The fact that the CO uptake after regeneration is similar to that of the fresh sample suggests that the original properties of the alloy can be restored to a certain degree, making the metal phase relatively stable.

Regarding acidity measurement, NH<sub>3</sub>-TPD characterization of the used 20CP450 catalyst showed an increased amount of high temperature sites (Fig. 9b)). This increased acidity might be attributed to the adsorption of reaction intermediates or the presence of carbonaceous species [45]. However, the fact that those high temperature acid sites were also present in the regenerated sample (used, calcined and reduced) suggest that those strong acid site might be related to unreduced Ni species (oxides or aluminates), which are more abundant due to the repeated thermal treatment (Fig. 8b)), that can act as Lewis acid sites [27]. Interestingly, the fact that the surface active sites concentration of neither functionalities decreased despite the detected carbon deposits suggests that the observed deactivation might be related to steric impediments exerted by the carbon deposits [46] which did not affect the prove molecules due to their significantly lower size compared to the reactants and products. Similarly to the 20CP450 sample, on the 20CP600 an increase in the high temperature acidity was observed. When the used 20CP600 sample was regenerated the acidity drastically dropped across all the temperature range but more acutely in the high temperature range (Table 5). This dramatic decrease in the acidity of the catalyst was most probably caused by a structural change [47] leading to a less hydroxylated surface with a much lower acidity.

According to the previous discussion, balanced amounts of adjacent metallic and acid sites are required for the reaction. Therefore,

considering that the amount of metallic active sites remains basically stable (Table 5) and the nature of the metallic species does not vary drastically (Fig. 8b)), the drop on acidity would damage the metallic – acid site relation and their distribution. In addition, electronic microscopy images showed Ni agglomeration on the regenerated 20CP600 catalyst, which would also be detrimental for the catalytic activity.

In good agreement with the other presented characterization techniques, microscopy images showed no meaningful modifications on the regenerated 20CP450 catalyst compared with the fresh sample (Fig. 10). However, as depicted in Fig. 7 some deactivation takes place on the 20CP450 catalyst between the first and the second run. The reason for this behavior can be found on the TPR profile showed in Fig. 8b). The variation on the profile, provably caused by the increased metal support interactions promoted during the repeated calcination processes, suggests modifications on the metal particles or their interaction, which could be the reason for the activity decrease evidenced in Fig. 7II. Besides, these processes also trigger the formation of hardly reducible NiAl<sub>2</sub>O<sub>4</sub> species [48], as observed in the TPR profiles of both 20CP450 and 20CP600 catalysts.

#### 4. Conclusions

The Ni-Cu-Al<sub>2</sub>O<sub>3</sub> catalytic system was thoroughly studied for the conversion of GVL into MTHF, finding major activity differences related to both the total metal content and the catalyst preparation method. Wet impregnation catalysts evidenced that their activities depend more on the metal phase nature than on the metal sites dispersion. In this catalysts series the higher activity (overall and as NMP) was shown by the catalysts with the lowest total concentration of metal active sites. The reason for that lies on the higher concentrations of Ni-Cu alloy related active sites that were promoted when high metal loadings were incorporated. In addition to this effect, catalyst acidity was found to play an important role; the activity of catalysts with the highest amounts of the active Ni-Cu alloy was limited by the lower acidity of these samples. Enhanced activities were achieved by using a co-precipitation preparation method, which further promotes Ni-Cu interactions, produces a more acidic material and enables a closer proximity between both

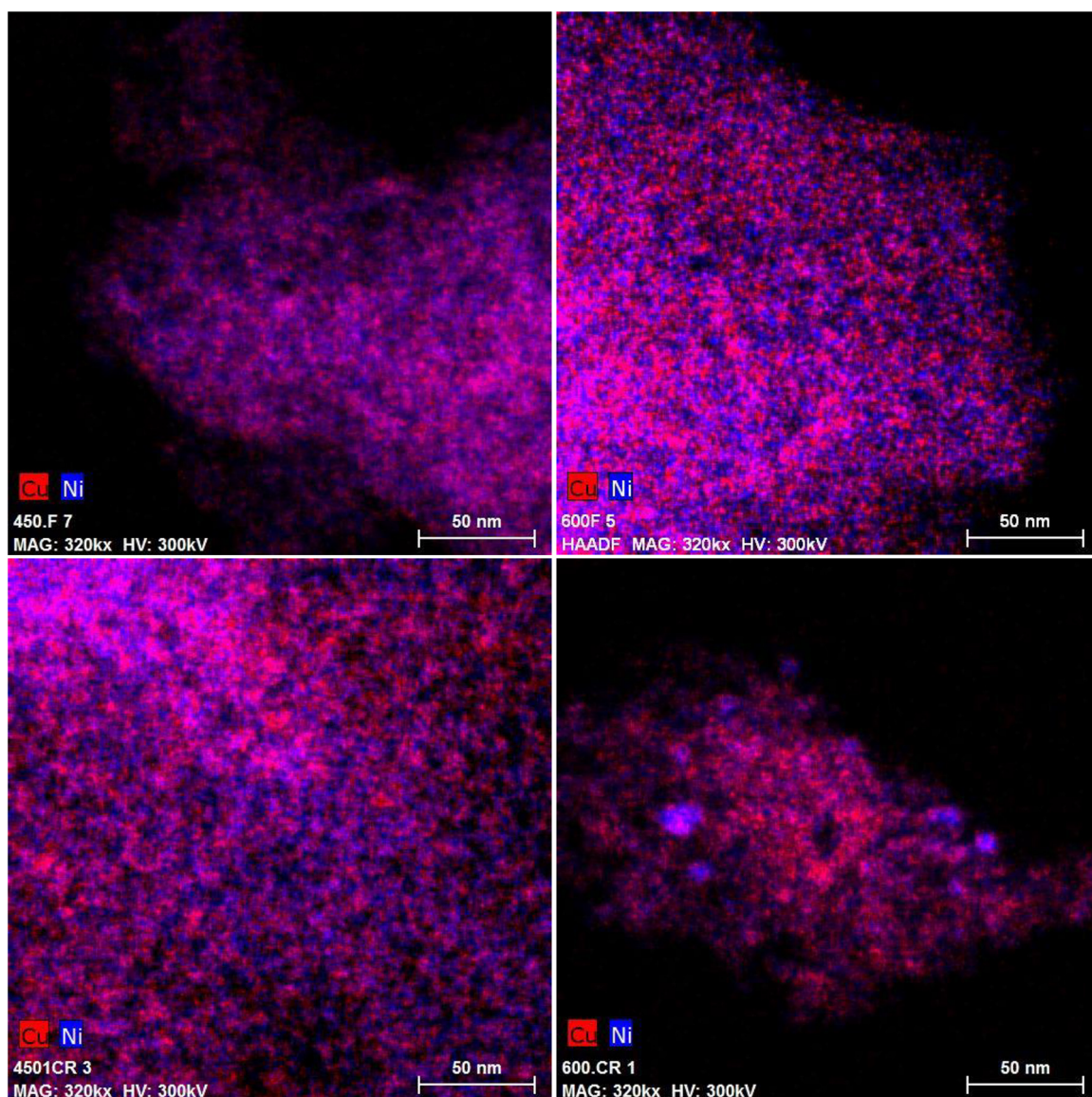


**Fig. 10.** STEM images of fresh (upper row) and regenerated (lower row) CP450 (left) and CP 600 (right) catalysts.

functionalities on the catalytic surface. Additional activity improvements were achieved on the co-precipitated catalyst by increasing the calcination temperature, reaching up to 64% MTHF yield after 5 h reaction time. The stability of these catalysts was evaluated and deactivation due to carbon deposition was found. Nevertheless, this activity loss can be attenuated by calcination and reduction (regeneration) between runs. This strategy allowed for a steady >54% MTHF yield after 3 runs for the most active catalysts, prepared by co-precipitation, while stable <36% MTHF yields were achieved for the impregnated catalyst.

## Acknowledgements

This work was supported by the UPV/EHU, Spanish Ministry of Economy and Competitiveness-FEDER (Project Ref. CTQ2015-64226-C3-2R), the Basque Government Predoc Training Programme, Department of Education and University (Project Ref. GIC 10/31 University). The authors thank for technical and human support provided by SGIker of UPV/EHU and European funding (ERDF and ESF).

## Appendix.

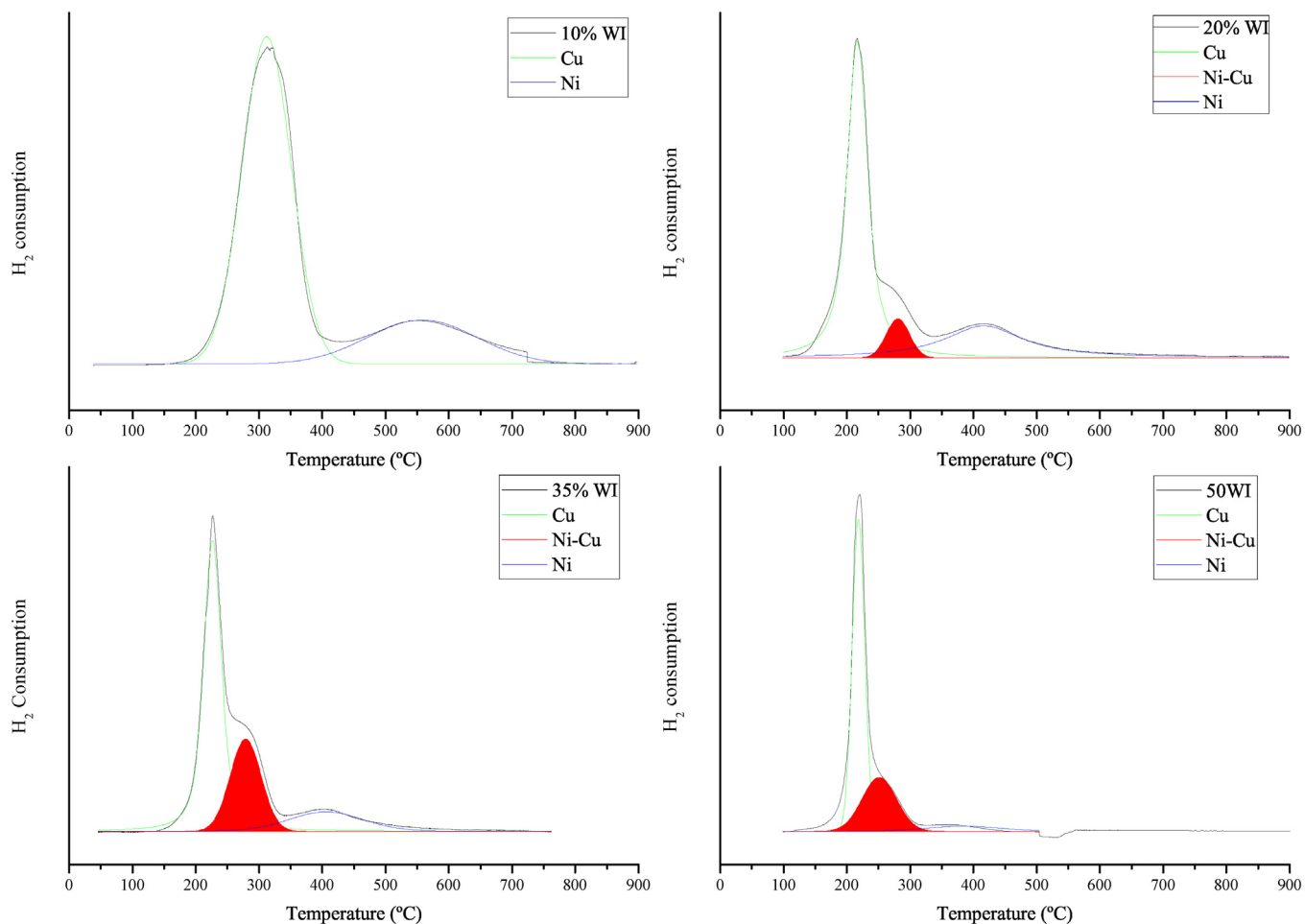


**Fig. A1.** TPR profiles and peak fitting for the WI catalyst series with different metal loadings.

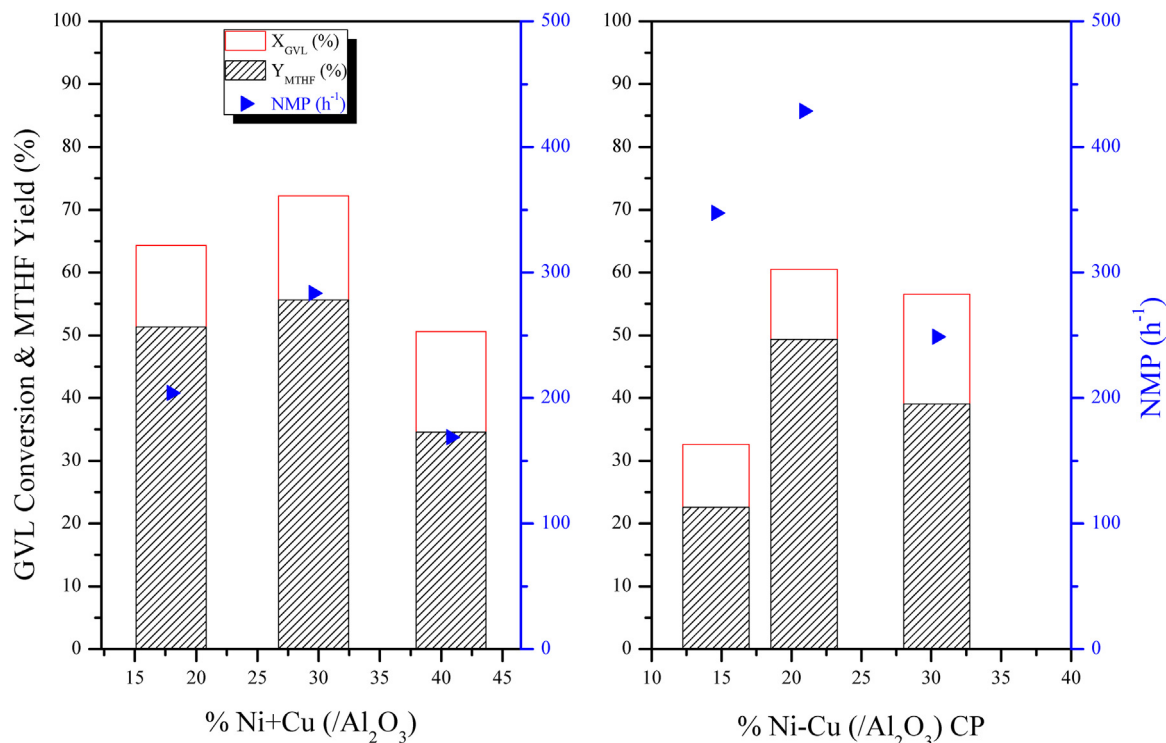


**Fig. A2.** Metal content screening for the Ni + Cu sequential impregnation and the CP methods.

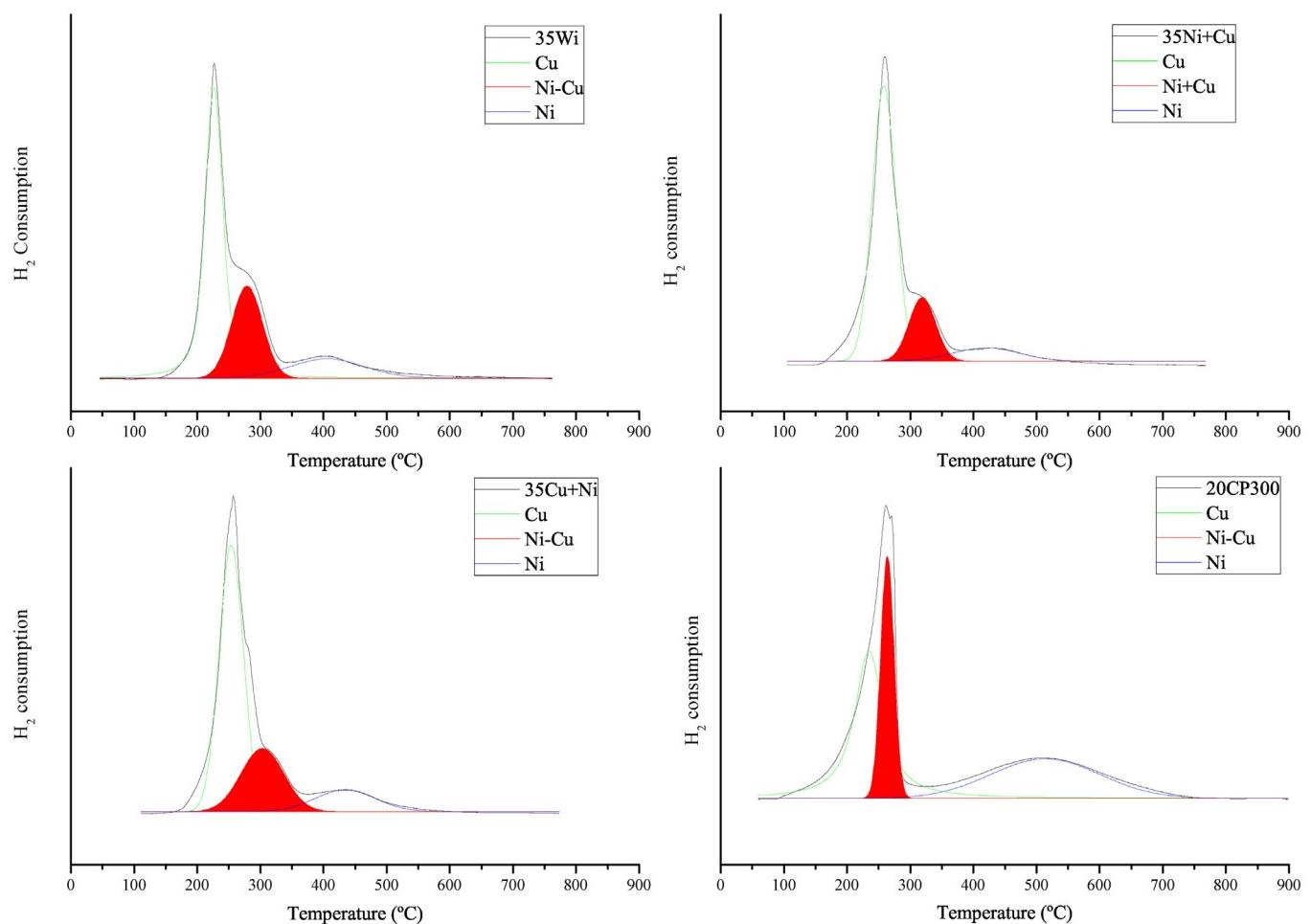


**Fig. A3.** TPR profiles and peak fitting for the 35% impregnation catalyst and the 20CP catalyst.

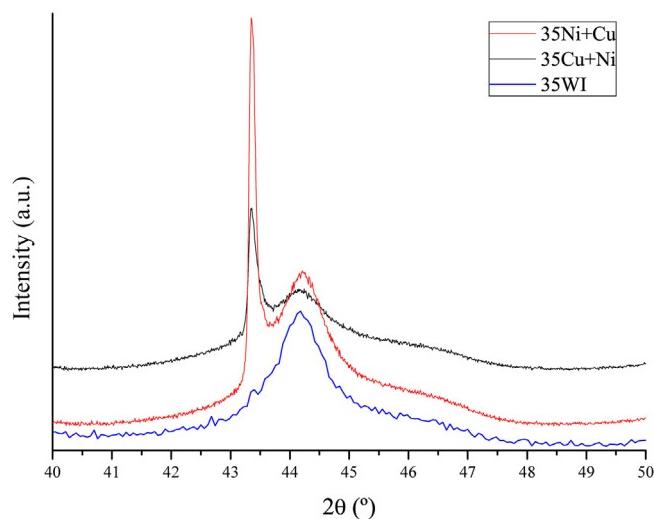


**Fig. A4.** High resolution XRD profiles of the three 35% impregnation catalysts.

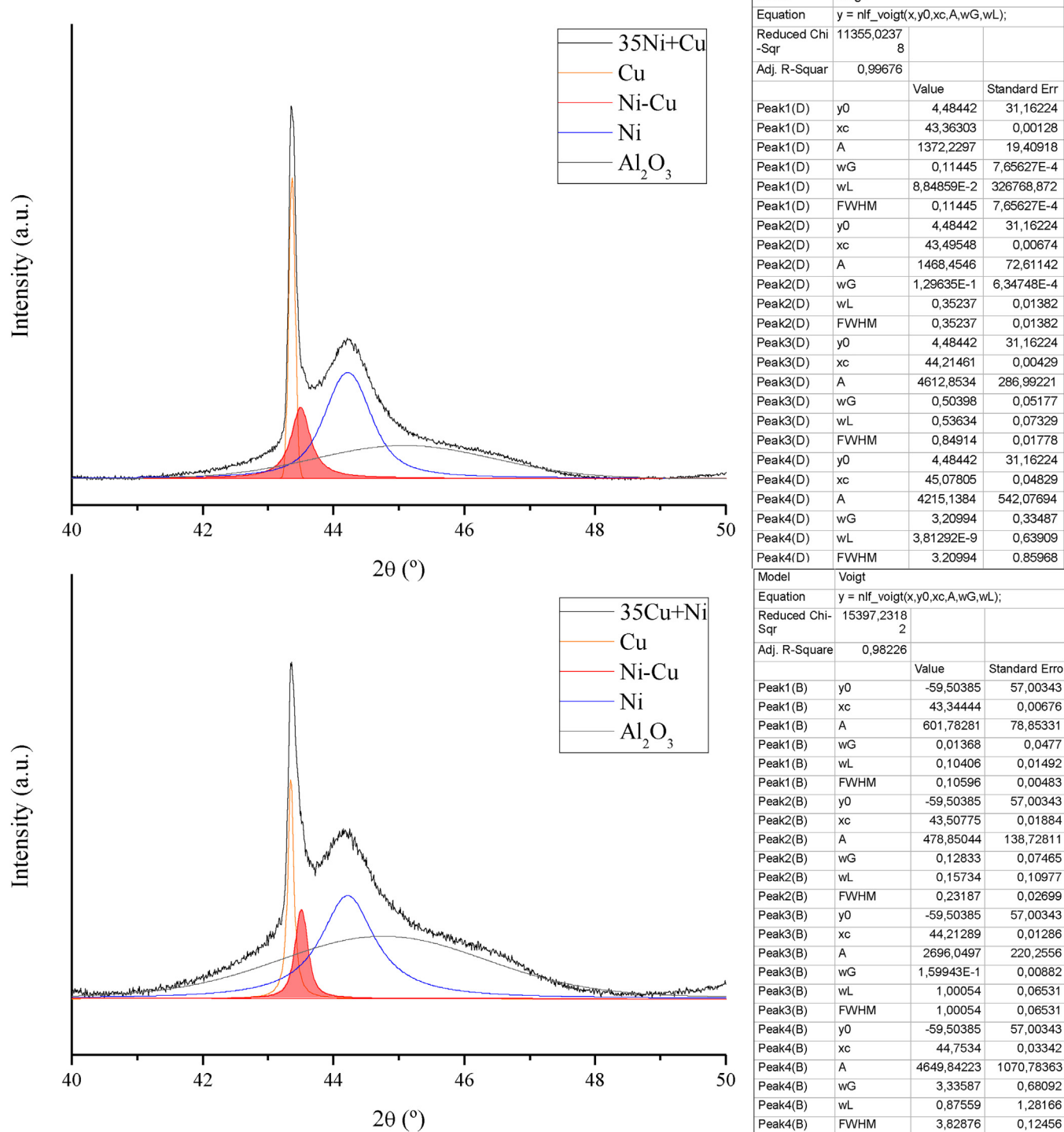


**Fig. A5.** High resolution XRD profile fitting of the 35Ni + Cu and 35Cu + Ni catalysts.

## References

- [1] British Petroleum, BP Statistical Review of World Energy, London, 2015.
- [2] C.S. Slater, M.J. Savelski, D. Hitchcock, E.J. Cavanagh, *J. Environ. Sci. Heal. Part A* 51 (2016) 487–494.
- [3] D.J. Hayes, S.W. Fitzpatrick, M.H.B. Hayes, J.R.H. Ross, in: B. Kamm, P.R. Gruber (Eds.), *Biorefineries-Industrial Process. Prod.*, Wiley-VCH Verlag GmbH, 2006, 2017, pp. 139–164.
- [4] J.J. Bozell, G.R. Petersen, *Green Chem.* 12 (2010) 539–554.
- [5] D.M. Alonso, S.G. Wettstein, J.a. Dumesic, *Green Chem.* 15 (2013) 584.
- [6] I.T. Horváth, H. Mehdi, V. Fabos, L. Boda, L.T. Mika, *Green Chem.* 10 (2008) 238.
- [7] V. Pace, P. Hoyos, L. Castoldi, P. Domínguez De María, A.R. Alcántara, *ChemSusChem* 5 (2012) 1369–1379.
- [8] I. Obregón, E. Corro, U. Izquierdo, J. Requies, P.L. Arias, *Chinese J. Catal.* 35 (2014) 656–662.
- [9] I. Obregón, I. Gandarias, M.G. Al-Shaal, C. Mevissen, P.L. Arias, R. Palkovits, *ChemSusChem* 9 (2016) 2488–2495.
- [10] H. Mehdi, V. Fábos, R. Tuba, A. Bodor, L.T. Mika, I.T. Horváth, *Top. Catal.* 48 (2008) 49.
- [11] F.M.A. Geilen, B.B. Engendahl, A. Harwardt, W. Marquardt, J. Klankermayer, W. Leitner, *Angew. Chem. Int. Ed.* 49 (2010) 5510–5514.
- [12] A. Phanopoulos, A.J.P. White, N.J. Long, P.W. Miller, *ACS Catal.* 5 (2015) 2500–2512.

- [13] D.C. Elliott, J.G. Frye, Hydrogenated 5C Compound and Method of Making, US 5883266, 1999.
- [14] T. Mizugaki, K. Togo, Z. Maeno, T. Mitsudome, K. Jitsukawa, K. Kaneda, ACS Sustain. Chem. Eng. 4 (2016) 682–685.
- [15] P.P. Upare, J.-M. Lee, Y.K. Hwang, D.W. Hwang, J.-H. Lee, S.B. Halligudi, J.-S. Hwang, J.-S. Chang, ChemSusChem 4 (2011) 1749–1752.
- [16] X.-L. Du, Q.-Y. Bi, Y.-M. Liu, Y. Cao, H.-Y. He, K.-N. Fan, Green Chem. 14 (2012) 935.
- [17] I. Obregón, I. Gandarias, N. Miletic, A. Ocio, P.L. Arias, ChemSusChem 8 (2015) 3483–3488.
- [18] P.P. Upare, M. Jeong, Y. Kyu, D. Han, Y. Dok, D. Won, U. Lee, J. Chang, Appl. Catal. A Gen. 491 (2015) 127–135.
- [19] M. Li, G. Li, N. Li, A. Wang, W. Dong, X. Wang, Y. Cong, Chem. Commun. 50 (2014) 1414–1416.
- [20] T. Mizugaki, Y. Nagatsu, K. Togo, Z. Maeno, T. Mitsudome, K. Jitsukawa, K. Kaneda, Green Chem. 17 (2015) 5136–5139.
- [21] W. Luo, M. Sankar, A.M. Beale, Q. He, C.J. Kiely, P.C.A. Bruijnincx, B.M. Weckhuysen, Nat. Commun. 6 (2015) 6540.
- [22] D.C. Elliott, J.G. Frye, Hydrogenated 5-Carbon Compound and Method of Making, 1999, pp. 5883266.
- [23] E.I. Gürbüz, D.M. Alonso, J.Q. Bond, J.a. Dumesic, ChemSusChem 4 (2011) 357–361.
- [24] X.L. Du, Q.Y. Bi, Y.M. Liu, Y. Cao, K.N. Fan, ChemSusChem 4 (2011) 1838–1843.
- [25] S.M. Sen, E.I. Gürbüz, S.G. Wettstein, D.M. Alonso, J.a. Dumesic, C.T. Maravelias, Green Chem. 7 (2012) 3289–3294.
- [26] P.G. Savva, K. Goundani, J. Vakros, K. Bourikas, C. Fountzoula, D. Vattis, a. Lycourghiotis, C. Kordulis, Appl. Catal. B Environ. 79 (2008) 199–207.
- [27] Z. Si, D. Weng, X. Wu, Z. Ma, J. Ma, R. Ran, Catal. Today 201 (2013) 122–130.
- [28] J. Ashok, M. Subrahmanyam, A. Venugopal, Int. J. Hydrogen Energy 33 (2008) 2704–2713.
- [29] I. Gandarias, J. Requieres, P.L. Arias, U. Armbruster, A. Martin, J. Catal. 290 (2012) 79–89.
- [30] E.T. Saw, U. Oemar, X.R. Tan, Y. Du, A. Borgna, K. Hidajat, S. Kawi, J. Catal. 314 (2014) 32–46.
- [31] A. Martin, U. Armbruster, I. Gandarias, P.L. Arias, Eur. J. Lipid Sci. Technol. 115 (2013) 9–27.
- [32] M. Haruta, Angew. Chem. Int. Ed. 53 (2014) 52–56.
- [33] G.W. Graham, H.W. Jen, O. Ezekoye, R.J. Kudla, W. Chun, X.Q. Pan, R.W. McCabe, Catal. Lett. 116 (2007) 1–8.
- [34] M.J. Gilkey, B. Xu, ACS Catal. 5 (2016) 1420–1436.
- [35] P. Barbieri, A. de Sierra, M. Carrazolle, R. Landers, G. Kleiman, J. Electron Spectrosc. Relat. Phenomena 135 (2004) 113–118.
- [36] A. Yin, C. Wen, X. Guo, W.-L. Dai, K. Fan, J. Catal. 280 (2011) 77–88.
- [37] A.R. Naghash, T.H. Etzell, S. Xu, Chem. Mater. 18 (2006) 2480–2488.
- [38] W. Luo, U. Deka, A.M. Beale, E.R.H. van Eck, P.C.A. Bruijnincx, B.M. Weckhuysen, J. Catal. 301 (2013) 175–186.
- [39] V.V. Kumar, G. Naresh, M. Sudhakar, C. Anjaneyulu, S.K. Bhargava, J. Tardio, V.K. Reddy, A.H. Padmasri, A. Venugopal, RSC Adv. 6 (2016) 9872–9879.
- [40] X. Tang, H. Chen, L. Hu, W. Hao, Y. Sun, X. Zeng, L. Lin, S. Liu, Appl. Catal. B Environ. 147 (2014) 827–834.
- [41] J. Wang, S. Jaenicke, G.-K. Chuah, RSC Adv. 4 (2014) 13481–13489.
- [42] S.G. Wettstein, J.Q. Bond, D.M. Alonso, H.N. Pham, A.K. Datye, J.A. Dumesic, Appl. Catal. B Environ. 117–118 (2012) 321–329.
- [43] S.T. Oyama, X. Wang, Y.-K. Lee, W.-J. Chun, J. Catal. 221 (2004) 263–273.
- [44] I. Simakova, O. Simakova, P. Mäki-Arvela, A. Simakov, M. Estrada, D.Y. Murzin, Appl. Catal. A Gen. 355 (2009) 100–108.
- [45] X. Tang, Z. Li, X. Zeng, Y. Jiang, S. Liu, T. Lei, Y. Sun, L. Lin, ChemSusChem 8 (2015) 1601–1607.
- [46] M. Guisnet, P. Magnoux, D. Martin, Stud. Surf. Sci. Catal. 111 (1997) 1–19.
- [47] L.A. O'Dell, S.L.P. Savin, A.V. Chadwick, M.E. Smith, Solid State Nucl. Magn. Reson. 31 (2007) 169–173.
- [48] F. Mariño, G. Baronetti, M. Jobbagy, M. Laborde, Appl. Catal. A Gen. 238 (2003) 41–54.